Continental Shelf Research 166 (2018) 83–91

Contents lists available at ScienceDirect

Continental Shelf Research

journal homepage: www.elsevier.com/locate/csr

Groundwater-surface water exchanges and associated nutrient fluxes in Dan'ao Estuary, Daya Bay, China

Gang Li[a,b,d], Hailong Li[b,c,*], Xuejing Wang[c], Wenjing Qu[a,b], Yan Zhang[a,b], Kai Xiao[a,b], Manhua Luo[c], Chunmiao Zheng[c]

[a] MOE Key Laboratory of Groundwater Circulation & Environmental Evolution, China University of Geosciences, Beijing 100083, China
[b] State Key Laboratory of Biogeology and Environmental Geology, China University of Geosciences, Beijing 100083, China
[c] School of Environmental Science & Engineering and Shenzhen Key Laboratory of Soil & Groundwater Pollution Control, Southern University of Science and Technology, Shenzhen 518055, China
[d] China Institute for Geo-Environmental Monitoring, Beijing 100081, China

ARTICLE INFO

Keywords:
Groundwater-surface water exchanges
Submarine groundwater discharge (SGD)
Fresh groundwater recharge
Nutrient fluxes
Mangrove swamp
Estuary

ABSTRACT

Based on field measurements from two typical intertidal transects at Dan'ao Estuary, groundwater-surface water and associated nutrient exchanges are quantified. Both groundwater discharge rate (39.1 ± 7.0 cm d^{-1}) and surface water inflow rate (7.7 ± 1.4 cm d^{-1}) at the upstream mangrove swamp transect are much higher than those (1.6 ± 0.3 and 2.1 ± 0.4 cm d^{-1}, respectively) at the downstream bare flat one. This large difference leads to their contrasting nitrogen forms. Much higher water exchange rates at the upstream transect generate much higher net dissolved inorganic nitrogen (DIN, including NH_4^+, NO_2^-, and NO_3^-), dissolved inorganic phosphorus (DIP), and dissolved silicate (DSi) fluxes (− 160.3 ± 39.2, − 14.6 ± 2.7, − 38.6 ± 7.0 mmol m^{-2} d^{-1}, respectively) than those (2.9 ± 0.9, − 0.08 ± 0.03, 1.1 ± 0.4 mmol m^{-2} d^{-1}, respectively) at the downstream one. The mangrove swamp at the upstream transect discharges substantial groundwater and associated nutrients to the estuary. The net nutrient loads by water exchange in this estuary can reach 23.5–78.7% of those by local river discharge.

1. Introduction

Estuaries are one of the world's most dynamic ecosystems, possessing irreplaceable environmental effects and socio-economic value (Rengarajan and Sarma, 2015). Submarine groundwater discharge (SGD) is an important pathway for the delivery of nutrients and pollutants into the estuaries (Burnett et al., 2001; Russoniello et al., 2013), and it can adjust the estuarine biogeochemical cycle (Harvey and Odum, 1990). Driven by both terrestrial and marine forces, SGD comprises submarine fresh groundwater discharge (SFGD) and recirculated saline groundwater discharge (RSGD), both of which can deliver chemicals to the ocean (Taniguchi et al., 2002). Although the relative proportion of SFGD is small, it can carry abundant new materials from land to the coastal oceans (Liu et al., 2017). Thus, SFGD affects the balances of water and materials in the aquifer system. Due to the complex temporal and spatial variations in environmental conditions, the estimation of the groundwater-surface water exchange flux is difficult, particularly in estuarine tidal flats (Sakamaki et al., 2006). Previous studies showed that nutrient concentrations are often higher in coastal groundwater than in rivers (Valiela et al., 1990; Moore, 1999; Charette and Buesseler, 2004; Kroeger et al., 2007; Ganju, 2011). In some estuaries and bays, nutrient fluxes carried by SGD exceed those from rivers, greatly influencing coastal marine nutrient cycling and primary productivity (Moore et al., 2002; Garrison et al., 2003; Slomp and Van Cappellen, 2004).

There are many studies to assess groundwater-surface water and associated nutrient exchanges using different methods, such as generalized Darcy's Law (Ma et al., 2015; Hou et al., 2016; Qu et al., 2017), radium and radon mass balances (Krest et al., 2000; Charette and Buesseler, 2004; Charette, 2007), seepage meters, water-salt budget and thermal infrared imagery (Giblin and Gaines, 1990; Portnoy et al., 1998). However, at estuaries, few studies have combined groundwater-surface water exchanges and associated nutrient fluxes through the groundwater-surface water interfaces. Here we made such an attempt to explore the effects of groundwater-surface water exchanges on the nutrient fluxes along two intertidal transects at the estuary of Dan'ao River, the largest river flowing into Daya Bay. Groundwater hydraulic heads and salinity dynamics were monitored using observation pair-

* Corresponding author at: State Key Laboratory of Biogeology and Environmental Geology, China University of Geosciences, Beijing 100083, China.
E-mail address: hailongli@cugb.edu.cn (H. Li).

https://doi.org/10.1016/j.csr.2018.06.014
Received 7 January 2018; Received in revised form 18 June 2018; Accepted 25 June 2018
Available online 26 June 2018

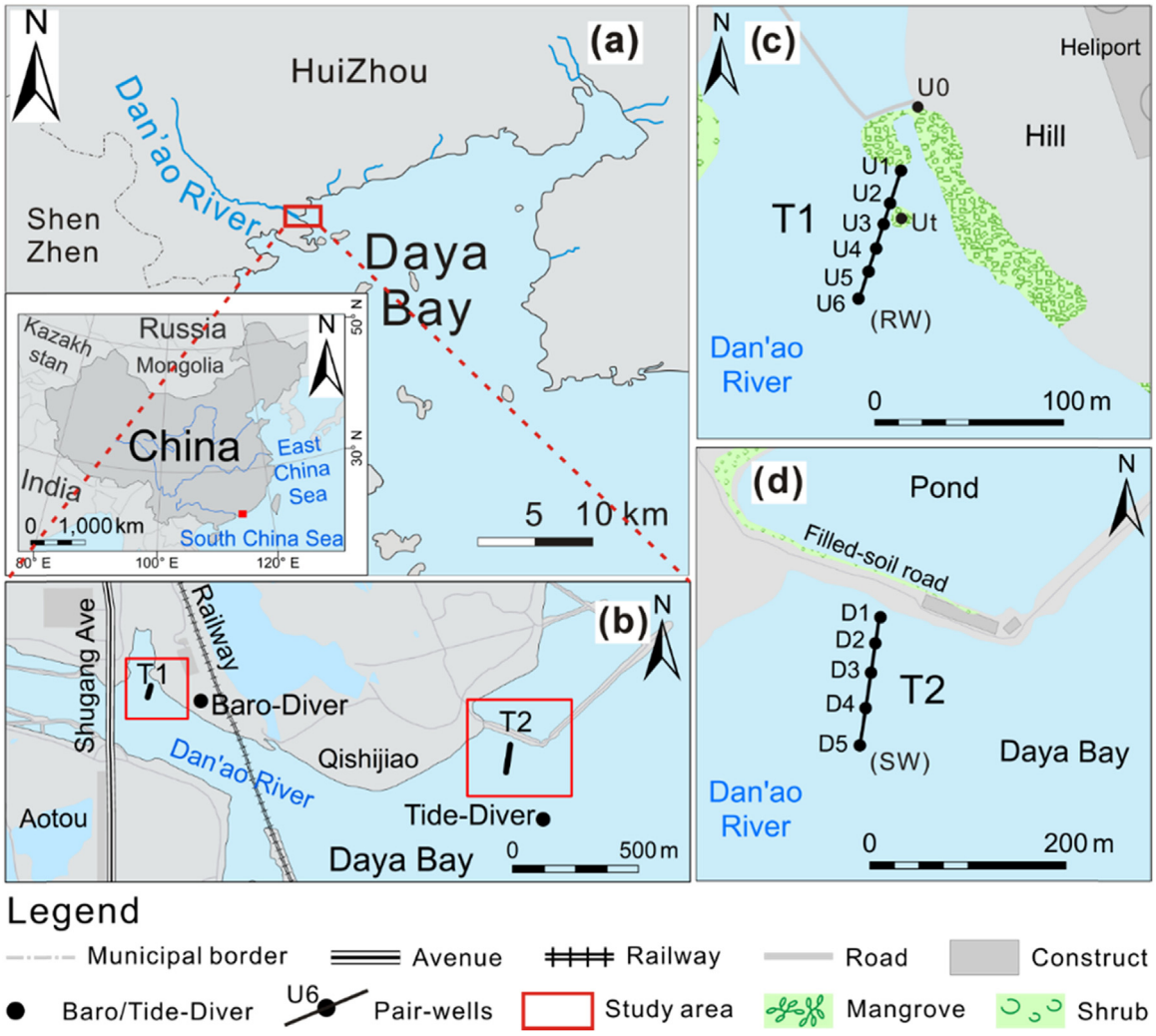

Fig. 1. Locations of the study site and observation wells.

wells installed at two different depths reported by Hou et al. (2016) and Qu et al. (2017). Groundwater at well locations and surface water at each transect were collected during the low tide. The concentrations of DIN, DIP, and DSi, were analyzed and compared. The groundwater-surface water exchange rates and associated nutrient fluxes were estimated and compared between the two transects.

2. Methodology

2.1. Study site and fieldwork

Daya Bay, a semi-enclosed bay, is located in the southeast of China (Fig. 1a). The climate belongs to a subtropical oceanic climate. Twelve small tidal rivers (flow rates $< 10\,m^3\ s^{-1}$) flow into the bay. The Dan'ao River is the largest one among them, which is ~ 10 km long with a discharge of 2.62–7.18 $m^3\ s^{-1}$ (Ren et al., 2013). The width of the river at the upstream and downstream transect is ~ 300 m and ~ 900 m, respectively (Fig. 1b). The study site is dominated by irregular semidiurnal tides, with a maximum tide range of ~ 2 m (Wu et al., 2017). Field measurements were conducted along two transects from December 16th 12:00 to December 24th 12:00, 2015. The mean tide range was 1.9 m during our fieldwork period. Two transects perpendicular to the river bank were deployed in the upstream and downstream intertidal wetlands. The distance between them was about 1.5 km (Fig. 1b).

The upstream transect (hereinafter referred to as T1) extended 62.1 m from the margin of mangroves to the low tide line. Six observation pair-wells (U1, …, U6) were set along the upstream transect (Fig. 1c). Each pair-wells contain two LTC-Divers (Level, Temperature and Conductivity Diver; Model 3001, LTC Levelogger® Junior, Solinst® Canada Ltd.) installed at two different depths with a fixed vertical distance of 0.528 m. Additionally, two other observation wells named U0 and Ut were installed at the upstream transect. The well U0 was located behind the mangroves at the hill foot to monitor the inland groundwater. The well Ut was imbedded in mangrove sediments beside U2 and U3 to monitor the groundwater around mangrove rhizosphere (Fig. 1c). The downstream transect (hereinafter referred to as T2) extended 120.5 m from the embankment foot to the riverbed. Five pair-wells (D1, …, D5) were set along the transect T2 (Fig. 1d). Simultaneously a Baro-Diver was installed near T1 to record the air pressure, and an LTC-Diver was installed beneath the low tide line near T2 to record tidal levels (Fig. 1b).

Pair-wells were installed at both transects to record groundwater head, electrical conductivity and temperature variations (Fig. 2). The transect topography and relative elevations of pair-wells were surveyed by a total station and the data are shown in Table 1. The vertical hydraulic conductivities K_v of the sediments were determined by in-situ multi-diameter falling-head method proposed by Wang et al. (2014) and the values are also listed in Table 1. The K_v-values were not measured at the most riverward wells U6 and D5 and they are approximated by the values in sediments around the wells U5 and D4, respectively.

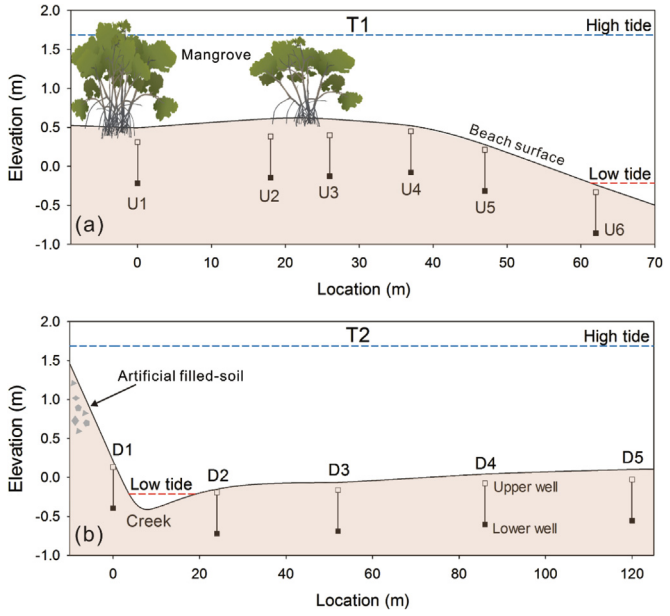

Fig. 2. Vertical cross-sections and locations of observation wells at the (a) upstream and (b) downstream transects.

Table 1
Locations and elevations of beach surface and wells, and the K_v values obtained by the in-situ falling-head method.

Pair-well no.	Location X_i (m)	Surface elevation (m)	Upper well elevation (m)	Mean K_v ($\times 10^{-5}$ m s^{-1})
U1	0	0.495	0.312	5.81
U2	17.8	0.613	0.384	2.88
Ut	–	–	–	0.17
U3	25.9	0.609	0.4	7.35
U4	36.8	0.522	0.45	0.04
U5	47.5	0.279	0.213	1.97
U6	62.1	− 0.236	− 0.329	1.97
D1	0	0.210	0.132	2.54
D2	24.4	− 0.153	− 0.193	0.18
D3	52.9	− 0.065	− 0.163	4.29
D4	86.9	0.042	− 0.077	0.64
D5	120.5	0.102	− 0.028	0.64

Note: The most landward well was set as the origin of X-coordinate for each transect (U1 for T1 and D1 for T2). The elevation datum for both transects is set as the top of D5 upper well.

2.2. Estimation of SGD and inflow

With the measurements of groundwater heads and salinities from the observation wells (See Appendix), the groundwater-surface water exchange rates are obtained based on the generalized Darcy's Law. The vertical flow rate q_i (in unit of cm d^{-1}) at the ith well is estimated by the following equation:

$$q_i \approx -\delta K_v \left[\frac{h_{up} - h_{low}}{\Delta L} + \frac{\varepsilon (c_{up} - c_{low})}{2} \right] \quad (1)$$

where K_v is the vertical hydraulic conductivity (m s^{-1}), h_{up} and h_{low} denote freshwater-equivalent hydraulic head (m) at the upper and lower LTC-Divers, respectively, ΔL is the distance between the upper and lower LTC-Divers and equals 0.528 m for all pair-wells, c_{up} and c_{low} denote the transformed salinity (g L^{-1}) of the pore water at the upper and lower LTC-Divers, respectively; ε is a constant equaling 7.143×10^{-4} m^3 kg^{-1}, which is used to describe the approximate linear relationship between density and transformed salinity, δ is the ratio of dynamic viscosity of freshwater to saltwater corresponding to the average salinities at the upper and lower LTC-Divers. For the transformation from salinity in unit of PSU (%) to that in unit of g L^{-1}, please refer to Ma et al. (2015). Since the variation range of the groundwater temperature is very limited (19.44–21.09 °C) in our case study, the influence of temperature on the groundwater density can be neglected and there is an approximate linear relationship between the density and transformed salinity. If $q_i > 0$, the groundwater will flow upwards into the surface water, and If $q_i < 0$, the surface water will flow downwards into the groundwater. Because of the rather gentle slopes and short lengths of the two transects, the horizontal groundwater-surface water exchanges are ignored in this study.

The rates (in unit of cm d^{-1}) of outflow SGD_i and inflow $Inflow_i$ at the ith well averaged over the entire observation period are then calculated using the following equations:

$$SGD_i = \frac{1}{t_e - t_0} \int_{t_0}^{t_e} \max_t [0, q_i(t)] dt \quad (2a)$$

$$Inflow_i = \frac{1}{t_e - t_0} \int_{t_0}^{t_e} \max_t [0, -q_i(t)] dt \quad (2b)$$

where t_0 is the initial time ($t_0 = 0$ h was set at 12:00 on December 19th, 2015); t_e is the end time ($t_e = 120$ h, corresponding to 12:00 on December 24th, 2015). The total SGD and $Inflow$ along the transect can be evaluated as follows:

$$SGD = \frac{1}{L} \sum_{i=1}^{n-1} \left(\int_{x_i}^{x_{i+1}} SGD_i dx \right) \quad (3a)$$

$$Inflow = \frac{1}{L} \sum_{i=1}^{n-1} \left(\int_{x_i}^{x_{i+1}} Inflow_i dx \right) \quad (3b)$$

where L denotes the considered transect length (m), n is the total number of pair-wells along the transect, x_i is the X-coordinate (m) of the ith well, ($i = 1, 2, \ldots, n$).

2.3. Water sampling and measurements

The shallow groundwater (at depths of shallow wells) and neighboring river water, seawater samples were collected simultaneously at both transects to measure nutrient concentrations during the low tide, on December 22nd, 2015. Here the nutrients measured include NH_4^+, NO_2^-, NO_3^-, DIN, DIP, and DSi. Groundwater was pumped using a peristaltic pump (Model 410, Solinst® Canada Ltd.) and a porewater sampler, PushPoint (M. H. E. Products, for details please refer to http://mheproducts.com/). Surface water was collected at riverward well U6 for T1 and D5 for T2. All water samples were collected in 50 ml sampling bottles, filtered in situ through 0.45 μm membrane filter, and stored under 4 °C in refrigerators until further measurements in the laboratory within three days. They were analyzed by spectrophotometer in National Research Center for Geoanalysis, Chinese Academy of Geological Sciences (CAGS). Based on the Specification for marine monitoring-Part 4: Seawater analysis by State Oceanic Administration of the People's Republic of China (2007), the methods for nutrient concentration measurements are as follows: Nessler reagent colorimetry for NH_4^+ (including NH_3) with an accuracy of 0.04 mg N L^{-1}, naphthyl ethylenediamine spectrophotometry for NO_2^- with an accuracy of 0.002 mg N L^{-1}, cadmium column reduction method for NO_3^- with an accuracy of 0.01 mg N L^{-1}, phosphorus molybdenum blue spectrophotometry for DIP with an accuracy of 0.005 mg L^{-1}, and silicon molybdenum yellow spectrophotometry for DSi with an accuracy of 0.02 mg L^{-1}.

2.4. Three-endmember mixing model

The estuarine shallow saline groundwater is the mixture of fresh water (including river water and fresh groundwater) and seawater.

Although silicate is a nutrient the concentration of which may be affected by biological uptake/release in seawater, which makes it non-conservative (Pilson, 1998; Millero, 2013), in comparison with DIN and DIP, DSi behaves more conservatively during the hydrological processes. Therefore, DSi is often used as a tracer to quantify the *SGD* in coastal waters like estuaries, lagoons and bays in many previous studies (Hwang et al., 2005, 2016; Ji et al., 2013; Rengarajan and Sarma, 2015; Luo and Jiao, 2016). Its concentrations differed in fresh groundwater, river water and seawater samples. Combining both tracers of salt and silicon, the seawater, river water and fresh groundwater fractions can be determined using the following three-endmember model:

$$F_{sw} + F_{rw} + F_{fg} = 1 \tag{4a}$$

$$F_{sw}S_{sw} + F_{rw}S_{rw} + F_{fg}S_{fg} = S_{gw} \tag{4b}$$

$$F_{sw}Si_{sw} + F_{rw}Si_{rw} + F_{fg}Si_{fg} = Si_{gw} \tag{4c}$$

where F_{sw}, F_{rw}, F_{fg} are the fractions (%) of seawater, river water, fresh groundwater, respectively, S_{sw} is the salinity (%) of seawater endmember, S_{rw} and S_{fg} are the salinities (%) of river water and fresh groundwater endmembers, respectively, S_{gw} is the salinity (%) of intertidal groundwater, Si_{sw}, Si_{rw}, Si_{fg} are the silicon concentration (μmol L^{-1}) of seawater, river water, and fresh groundwater endmembers, respectively, and Si_{gw} is the silicon concentration (μmol L^{-1}) of intertidal groundwater.

2.5. Determination of nutrient fluxes

The nutrient efflux f_{N_SGD} (in unit of mmol m^{-2} d^{-1}) carried by *SGD* and nutrient influx f_{N_Inflow} (mmol m^{-2} d^{-1}) carried by *Inflow* (seawater and river water) along each transect are estimated by the following equations:

$$f_{N\_SGD} = \frac{1}{2L}\sum_{i=1}^{n-1}(SGD_i c_i + SGD_{i+1}c_{i+1})d_{i.i+1} \tag{5a}$$

$$f_{N\_Inflow} = \frac{1}{2L}\sum_{i=1}^{n-1}(Inflow_i + Inflow_{i+1})c_{surface}\,d_{i.i+1} \tag{5b}$$

where $d_{i,i+1}$ is the horizontal distance (m) between the ith and $i+1$th pair-wells, c_i is the nutrient concentration (μmol L^{-1}) in intertidal groundwater at the depth of the upper well of the ith pair-well, $c_{surface}$ is the nutrient concentration (μmol L^{-1}) in river water or seawater at the transect. Therefore, the net nutrient flux f_{N_net} (mmol m^{-2} d^{-1}) in the intertidal groundwater at each transect can be estimated as follows:

$$f_{N\_net} = -f_{N\_SGD} + f_{N\_Inflow} \tag{6}$$

3. Results

3.1. Water exchange rates

The monitoring period averaged groundwater-surface water exchange rates at each well are obtained at both transects (Fig. 3). The water exchange rates (SGD_i and $Inflow_i$) at well locations along the upstream transect are mostly larger than those along the downstream one. The total *SGD* and *Inflow* along the upstream transect are estimated to be 39.1 and 7.7 cm d^{-1}, respectively; and the corresponding values along the downstream one are estimated to be 1.6 and 2.1 cm d^{-1}, respectively. It is found that the *SGD* along the upstream transect is much larger than its *Inflow*, which indicates a substantial fresh groundwater discharge of 31.4 cm d^{-1}. On the contrary, along the downstream transect, the *SGD* is very small, and less than its *Inflow*. Through the comparisons between the two transects, the *Inflows* along the two transects are on the same order of magnitude. However, the *SGD* along the upstream transect is ~12 times greater than that along the downstream one.

3.2. Nutrient data

The concentrations of nutrients (NH_4^+, NO_2^-, NO_3^-, DIN, DIP and DSi) in intertidal groundwater and surface water samples from the two transects are shown in Fig. 4. There are large differences in forms and concentrations of inorganic nitrogen between two transects. At the upstream transect, the DIN is dominated by NO_2^- and NH_4^+, while at the downstream one, the DIN is in the forms of NO_2^- and NO_3^-. At both transects, the NO_2^- accounts for the main part of the DIN. The concentration of NO_2^- (0.22–0.43 mmol L^{-1}) at the upstream transect is 3.8 times as high as those (0.09–0.22 mmol L^{-1}) at the downstream one. The reductive nitrogen form of NH_4^+ exists in groundwater at the four neighboring wells U2, Ut, U3, U4 (defined as Group A, and the remaining wells U0, U1, U5 are defined as Group B) at the upstream transect, while not detected at the downstream one. At the downstream transect, both groundwater and surface water contain detectable NO_3^-. However, at the upstream transect, only river water and groundwater at wells U0, U2 and U5 contain NO_3^-, with NO_3^- not detected in groundwater at other wells.

From Fig. 4, the mean concentrations of DIN, DIP and DSi in groundwater at the upstream transect are all higher than those at the downstream one. The nutrient concentrations in river water at the upstream transect are always higher than those in seawater at the downstream transect. Note that the *SGD* at the upstream transect is also much higher than that at the downstream one. Therefore, the higher concentrations of nutrients at the upstream transect may result from its higher *SGD*.

3.3. Three-endmember mixing ratios

To avoid the dilution by river water during the low tides, S_{sw} is set as 29.95 g L^{-1}, the mean salinity at high tides. The value of 0 g L^{-1} is adopted for both S_{rw} and S_{fg}. The salinity of intertidal groundwater (S_{gw}) averaged over the monitoring period at T1 is 18.78 g L^{-1}, and that at T2 is 24.01 g L^{-1}. The values of Si_{sw}, Si_{rw}, Si_{fg} are 0.05, 0.09, 0.24 mmol L^{-1}, respectively. The values of Si_{gw} are 0.11 mmol L^{-1} and 0.06 mmol L^{-1} for T1 and T2, respectively. Based on the above endmember values and the three-endmember mixing model (Eqs. (4a)–(4c)), seawater, river water and fresh groundwater fractions in intertidal groundwater at the upstream transect are estimated to be 62.7%, 7.2% and 30.1%, respectively (Fig. 5). At the downstream transect, the corresponding ratios are 80.2%, 18.5% and 1.4%, respectively. Note that the fresh groundwater fraction (30.1%) at the upstream transect is much higher than that (1.4%) at the downstream one, which indicates a great terrestrial fresh groundwater discharge at the upstream transect.

3.4. Estimation of nutrient fluxes

Based on Eqs. (1), (2a), (2b), (5a), (5b) and (6), the nutrient (DIN, DIP and DSi) fluxes through the water-sediment interfaces at the two transects are estimated and shown in Table 2 and Fig. 6. The estimations of DIN, DIP and DSi flux (− 160.3 ± 39.2, − 14.6 ± 2.7, − 38.6 ± 7.0 mmol m^{-2} d^{-1}, respectively) at the upstream transect are all greater than those (2.9 ± 0.9, − 0.08 ± 0.03, 1.1 ± 0.4 mmol m^{-2} d^{-1}, respectively) at the downstream one by 1–2 orders of magnitude. All nutrient species flow outwards from the water-sediment interface at the upstream transect, while they (except DIP) all flow into the groundwater at the downstream one. This indicates that the intertidal groundwater at the upstream transect acts as a major source of nutrients to the surface water in this estuary. On the contrary, at the downstream transect, the intertidal groundwater makes little difference on the nutrient fluxes, or just serves as a slight sink of nutrients. The above estimates are applied only to the days of sampling period in the dry season.

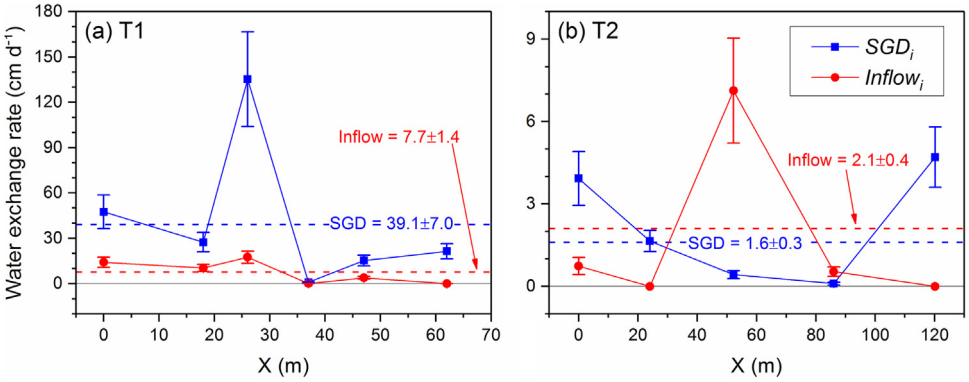

Fig. 3. Groundwater-surface water exchange rates averaged over the monitoring period at the (a) upstream and (b) downstream transects. Error bars represent standard deviations in the exchange rates determined by the measurement errors (see detailed discussion in Section 4.3).

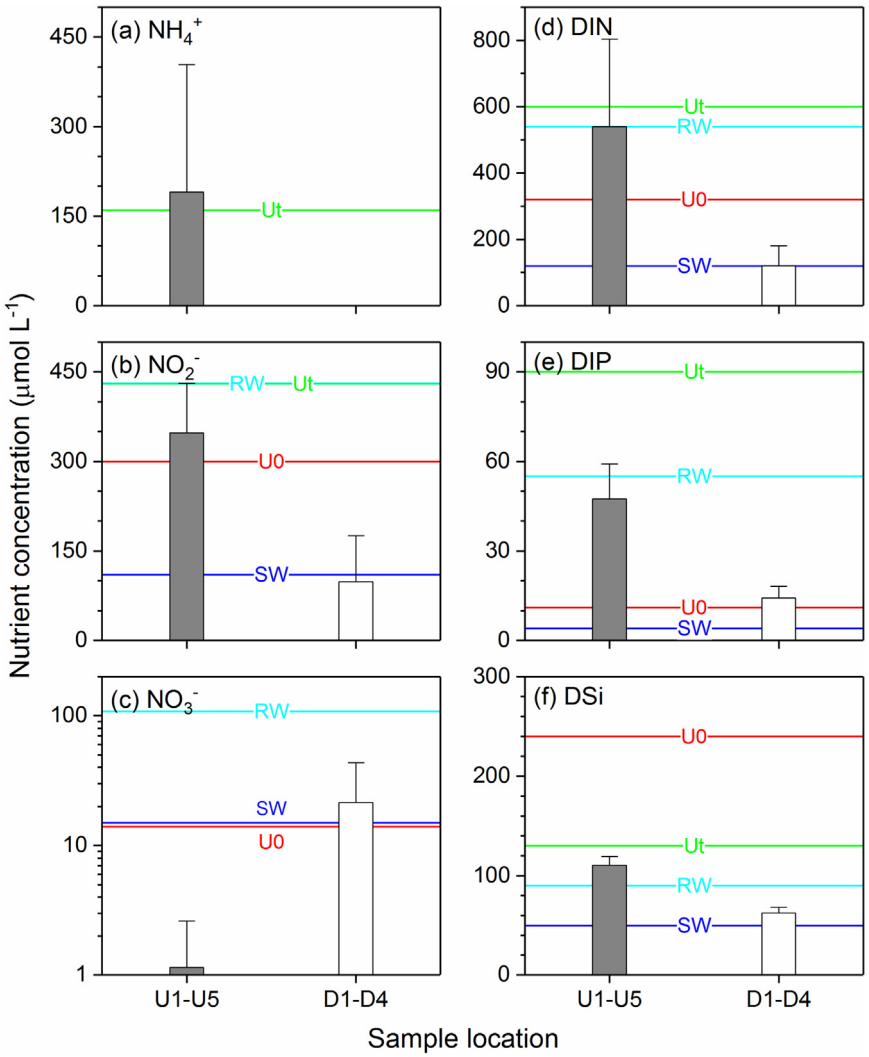

Fig. 4. Nutrient concentrations in intertidal groundwater at the two transects. The error bars indicate the standard deviation. The nutrient concentrations in groundwater at wells U0, Ut, river water (RW) and seawater (SW) are also shown for comparisons. Note that the NH_4^+ in U0, RW, SW and the NO_3^- in Ut are not detected.

4. Discussion

4.1. Comparison with previous studies

The *SGD*s, *Inflow*s and the effluxes of DIN and DIP at the two transects in this study are compared with those in previous studies and presented in Table 3, it is found that the *SGD* and *Inflow* along the downstream transect (1.6 ± 0.3 cm d^{-1} and 2.1 ± 0.4 cm d^{-1}, respectively) and upstream transect (39.1 ± 7.0 cm d^{-1} and 7.7 ± 1.4 cm d^{-1}, respectively) are among the value ranges of previous results (*SGD*: 0.71–77 cm d^{-1}, *Inflow*: 0.18–3.9 cm d^{-1}, based on the results from references in Table 3).

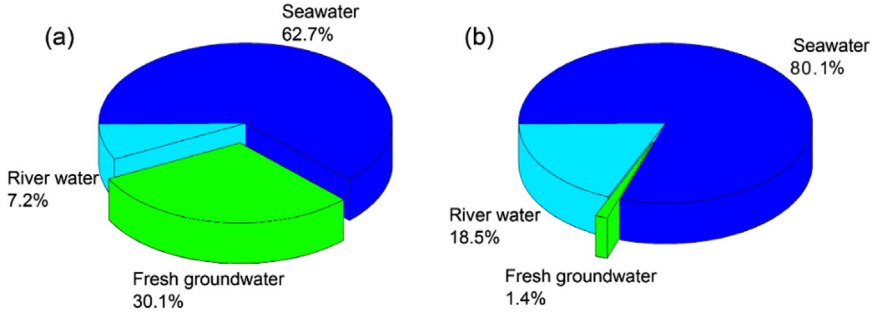

Fig. 5. Seawater, river water and fresh groundwater fractions in intertidal groundwater at the (a) upstream and (b) downstream transects.

The great differences in *SGD* and *Inflow* between the two transects may be mainly attributed to three aspects, namely geological, hydrological and ecological factors. Firstly, the larger slope of the hill leaned against by the upstream transect (Fig. 1c), can lead to a larger hydraulic gradient than that at the downstream one. The hill is mainly composed of red sandstone, which can store and transport sufficient rainfall. On the contrary, the topography is very flat at the downstream bare tidal transect (Fig. 1d). Secondly, the sediments at the upstream transect (mean $k_v = 2.9 \times 10^{-5}$ m s^{-1}) are more permeable than those at the downstream one (mean $k_v = 1.7 \times 10^{-5}$ m s^{-1}) (Table 1). Gleeson et al. (2013) and Sadat-Noori et al. (2017) found that mangrove environments within subtropical estuaries are hotspots for porewater exchange. Last but not least, it is inferred that the complicated network of mangrove roots may generate preferential pathways for water exchanges at the upstream transect.

The effluxes of DIN and DIP (2.2 ± 0.4 and 0.24 ± 0.04 mmol m^{-2} d^{-1}, respectively) at the downstream transect are comparable to those (DIN: 2.4–72 mmol m^{-2} d^{-1}, DIP: 0.004–1.48 mmol m^{-2} d^{-1}) reported in previous studies (Table 3). However, at the upstream transect, the effluxes of DIN (201.9 ± 36.3 mmol m^{-2} d^{-1}) and DIP (18.9 ± 3.4 mmol m^{-2} d^{-1}) are at least one order of magnitude higher than those reported in the previous studies (Table 3).

4.2. Nutrient loads by water exchange and river discharge

Nutrient loads by groundwater-surface water exchange and river discharge are two important nutrient sources for coastal waters. Wilson and Morris (2012) and Qu et al. (2017) concluded that increases in tidal amplitude can increase groundwater flushing in tidal salt marsh-dominated estuaries. Since the field work was conducted during the neap tide, larger water exchange rates should be observed during the spring tide when the river bed between T1 and T2 is wholly exposed in the air during low tides (according to the statement by local fishers on our field trip). Thus, the water exchange area between T1 and T2 can reach a value of ~ 8.38×10^5 m^2. The values of f_{N_net} at the two transects are averaged to gain a reasonable nutrient load estimation for the monitoring period. The net nutrient load (L_{N_net}, mol d^{-1}) by water exchanges is estimated by the product of the mean f_{N_net} and the water exchange area.

$$L_{N\_net} = -\overline{f_{N\_net}} \times A_{T1\sim T2} \quad (7)$$

Where $\overline{f_{N\_net}}$ is the averaged value of f_{N_net}-s at the upstream and downstream transects, and $A_{T1\sim T2}$ is the water exchange area of the estuary section between the two transects.

The nutrient flux by river discharge (L_{N_rw}) is determined by the following equation:

$$L_{N\_rw} = \overline{Q_{rw}} \times c_{rw} \quad (8)$$

where Q_{rw} is the river flow rate (m^3 d^{-1}), with an average value of 3.14×10^5 (Wang et al., 2018), and c_{rw} is the nutrient concentration in river water.

The results of L_{N_net}, L_{N_rw} and the L_{N_net}/L_{N_rw} ratios in this dry season are shown in Table 4. It is found that the nutrient loads by water exchange in the estuary section between T1 and T2 account for 23.5–78.7% of those by the local river discharge, which is a relatively high proportion, given that the length (~ 1.5 km) of the considered river section is only ~ 15% of the total river length.

4.3. Uncertainty analysis

Based on the methodology section, the uncertainty for the estimations of water exchange rates and associated nutrient fluxes may come from the measurement errors of water heads (h_{up}, h_{low}), salinities (c_{up}, c_{low}) by LTC-Divers, hydraulic conductivities (K_v), distances/lengths

Table 2
Estimates of groundwater–surface water exchange rates at each well location, water exchange fluxes and associated nutrient fluxes along each transect.

Well number	Water exchange rate (cm d^{-1})		Nutrient concentration c_i or $c_{surface}$ (μmol L^{-1})			Transect segment	Distance $d_{i,i+1}$ (m)	Transect and length L (m)	Water flux (cm d^{-1})	Nutrient flux (mmol m^{-2} d^{-1})		
	SGD_i	$Inflow_i$	DIN	DIP	DSi					DIN	DIP	DSi
U1	47.5 ± 8.6	14.1 ± 2.6	217.4	51.6	107.7			T1 (62.1)		f_{N_SGD}:	f_{N_SGD}:	f_{N_SGD}:
U2	27.4 ± 4.9	10.4 ± 1.9	993.4	54.8	107.7	U1-U2	17.8		*SGD*:	− 201.9 ± 36.3	− 18.9 ± 3.4	− 45.7 ± 8.2
U3	135.4 ± 24.3	17.5 ± 3.2	525.9	51.6	127.0	U2-U3	8.2		39.1 ± 7.0	f_{N_Inflow}:	f_{N_Inflow}:	f_{N_Inflow}:
U4	0.9 ± 0.2	0.09 ± 0.02	608.8	54.8	110.3	U3-U4	10.9			41.6 ± 7.6	4.2 ± 0.8	7.1 ± 1.3
U5	15.3 ± 2.8	3.8 ± 0.7	350.0	24.2	99.3	U4-U5	10.6		*Inflow*:	f_{N_net}:	f_{N_net}:	f_{N_net}:
U6 (RW)	21.4 ± 3.9	0.009 ± 0.008	542.6	54.8	93.0	U5-U6	14.6		7.7 ± 1.4	− 160.3 ± 39.2	− 14.6 ± 2.7	− 38.6 ± 7.0
D1	3.9 ± 0.8	0.7 ± 0.2	62.3	9.5	68.7			T2 (120.5)		f_{N_SGD}:	f_{N_SGD}:	f_{N_SGD}:
D2	1.6 ± 0.3	0 ± 0	99.1	17.7	65.3	D1-D2	24.4		*SGD*:	− 2.2 ± 0.4	− 0.24 ± 0.04	− 1.0 ± 0.2
D3	0.4 ± 0.1	7.1 ± 1.5	96.2	11.4	53.0	D2-D3	28.5		1.6 ± 0.3	f_{N_Inflow}:	f_{N_Inflow}:	f_{N_Inflow}:
D4	0.10 ± 0.04	0.5 ± 0.1	222.4	18.5	63.0	D3-D4	34.0		*Inflow*:	5.2 ± 1.1	0.16 ± 0.03	2.1 ± 0.4
D5 (SW)	4.7 ± 0.9	0 ± 0	123.7	3.9	50.0	D4-D5	33.6		2.1 ± 0.4	f_{N_net}:	f_{N_net}:	f_{N_net}:

Note: the accuracies of nutrient concentrations (c_i and $c_{surface}$) and distance $d_{i\,i+1}$, transect length L are explained in Sections 2.3 and 4.3, respectively.

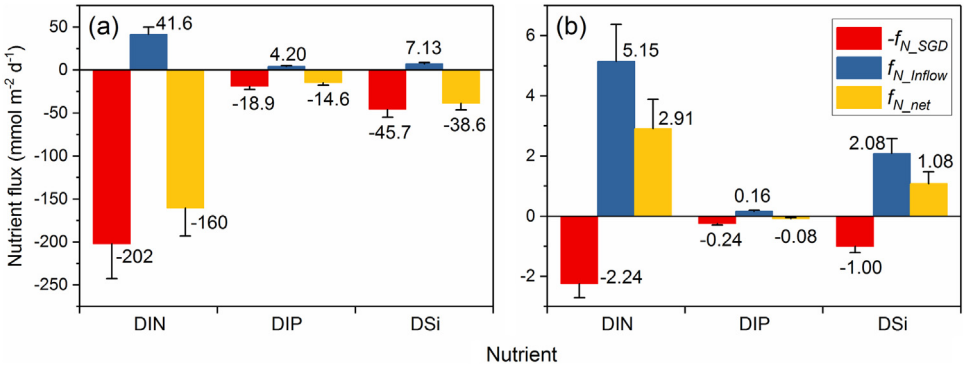

Fig. 6. Estimates of nutrient fluxes by *SGD*, by *Inflow*, and the net nutrient fluxes in intertidal groundwater at the (a) upstream and (b) downstream transects.

Table 3
Comparisons of *SGDs*, *Inflows* and effluxes of DIN, DIP between this study and previous ones.

Study site	***SGD*** (cm d^{-1})	***Inflow*** (cm d^{-1})	**DIN efflux** (mmol m^{-2} d^{-1})	**DIP efflux** (mmol m^{-2} d^{-1})	**Ref.**
Mangrove swamp, Dan'ao Estuary, China	39.1 ± 7.0	7.7 ± 1.4	201.9 ± 36.3	18.9 ± 3.4	This study
Bare tidal flat, Dan'ao Estuary, China	1.6 ± 0.3	2.1 ± 0.4	2.2 ± 0.4	0.24 ± 0.04	
Tidal flat, Laizhou Bay, China	2.24	3.90	n.a.	n.a.	Ma et al. (2015)
Silty tidal flat, Laizhou Bay, China	4.67	0.18	n.a.	n.a.	Hou et al. (2016)
Mangrove marsh, Yanfeng Estuary, China	2.21	n.a.	n.a.	n.a.	Xia and Li (2012)
Bald mud beach, Yanfeng Estuary, China	3.03	n.a.	n.a.	n.a.	
Mud flat, Jiaozhou Bay, China	0.71	1.01	7.4	0.004	Qu et al. (2017)
Sandy beach, Jiaozhou Bay, China	7.63	0.18	9.5	0.018	
Elizabeth Estuary, US	1.8–3.2	n.a.	4.5 ± 4.6	0.16 ± 0.17	Charette and Buesseler (2004)
North Inlet salt marsh, US	3.15	n.a.	2.42	0.91	Krest et al. (2000)
Salt marsh estuary, Pamet River, US	77	n.a.	4.7–19.5	0.36–1.48	Charette (2007)
Nauset marsh estuary, US	2.6–18	n.a.	24–72	n.a.	Portnoy et al. (1998), Giblin and Gaines (1990)
Tolo Harbor, Hong Kong, China	2.7–5.4	n.a.	2.9–6.7	0.02–0.11	Luo and Jiao (2016)
Bangdu Bay, Korea	43.6	n.a.	21.4 ± 3.2	0.16 ± 0.02	Hwang et al. (2005)

Note: n.a. denotes not available. Tolo Harbor and Bangdu Bay are on a similar scale of Dan'ao Estuary.

Table 4
Nutrient loads by water exchange and river discharge in the dry season.

Nutrient load (mol d^{-1})	**DIN**	**DIP**	**DSi**
L_{N_net}	(4.42–9.10) × 10^4	(4.45–7.95) × 10^3	(1.14–2.07) × 10^4
L_{N_rw}	(1.53–1.87) × 10^5	(1.55–1.89) × 10^4	(2.63–3.21) × 10^4
L_{N_net}/L_{N_rw}	23.6–59.4%	23.5–51.3%	35.3–78.7%

(ΔL, L, $d_{i,i+1}$) by the total station/steel tape, and nutrient concentrations (c_i, $c_{surface}$). According to Eqs. (7) and (8) in Section 4.2, the nutrient loads by water exchange and river discharge are also influenced by the estuarine area $A_{T1\sim T2}$ and river discharge rate Q_{rw}.

The accuracy of water head measured by LTC-Divers is within 0.1% of measurement range, according to the user guide of LTC-Divers by the Solinst manufacturer. The relative error of K_v caused by both the neglection of horizontal flow near the low end of the apparatus and the man-made observation errors is less than 10% (Wang et al., 2014; Qu et al., 2017). The LTC-Divers have an accuracy of 2% of readings in electric conductivity from the user guide of LTC-Divers by the Solinst manufacturer. This induced an error of < 2.5% when converting the electrical conductivity into the salt concentration (c_{up}, c_{low}). Further calculations show that the relative errors of *Inflow* and *SGD* caused by errors in salinity are no more than 3%. The length of pair-well link rod (ΔL), distance of adjacent well location ($d_{i,i+1}$), and transect length (L) were measured by a steel tape with an accuracy of 1 mm, leading to a relative error of less than 0.25% in estimating *Inflow* and *SGD*. For conservative estimations, here we magnify the relative error of K_v to be 20% to include the errors caused by salinities (c_{up}, c_{low}) and distances (ΔL, L, $d_{i,i+1}$) (Qu et al., 2017). The accuracies of nutrient concentrations (c_i, $c_{surface}$) are shown in Section 2.3. Compared with the nutrient measurements, the errors of DIN, DIP and DSi concentrations were less than 6.0%, 4.1% and 1.4%, respectively. To guarantee more reliable estimates of nutrient loads in Section 4.2, the errors of $A_{T1\sim T2}$ and Q_{rw} are assigned to be ~10%.

Considering all the measurement errors mentioned above, the final uncertainties of groundwater-surface water exchange rates and associated nutrient fluxes are shown in Fig. 3, Table 2 and Fig. 6. Taking into account all the uncertainties of above-mentioned ones and $A_{T1\sim T2}$, Q_{rw}, the final estimates of nutrient loads by water exchange and river discharge are compared and displayed in Table 4.

4.4. Water exchanges and nitrogen forms

The dominance of NO_2^- in DIN in estuarine waters from subterranean estuaries and surface estuaries is not common (An and Gardner, 2002; Charette and Buesseler, 2004; Akamatsu et al., 2009; Charette et al., 2013). One major reason for this unusual phenomenon may probably be the different chemical reactions occurring at the two transects, owing to their different water exchange rates. The sediments and groundwater in mangrove swamps is usually anaerobic and organic-matter rich (Reef et al., 2010). Thus, it is assumed that the much higher *SGD* at the upstream mangrove swamp (39.1 cm d^{-1}) than that

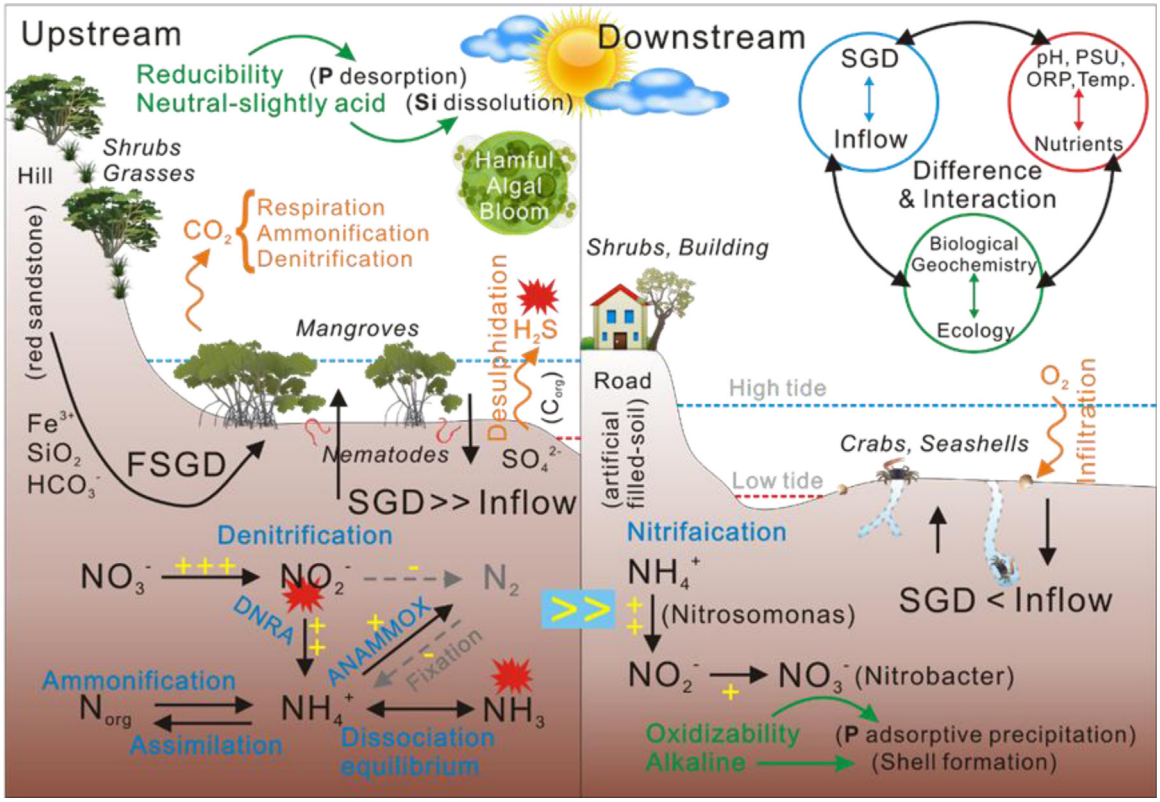

Fig. 7. Conceptual model of groundwater–surface water exchange and associated nutrient transformation at the two transects of Dan'ao Estuary.

of the downstream bare tidal flat (1.6 cm d^{-1}) contributed to the more reductive condition at the upstream transect. Due to the higher DO (dissolved oxygen) concentration in surface water than that in groundwater, the higher *Inflow* (2.1 cm d^{-1}) than *SGD* (1.6 cm d^{-1}) at the downstream transect indicates a more oxidative environment.

From the conceptual model of groundwater–surface water exchange and associated nutrient transformation (Fig. 7), we assumed that in the reductive environment at the upstream transect, the subprocess of NO_3^- → NO_2^- exceeded that of NO_2^- → NH_4^+ in both denitrification and DNRA (dissimilatory nitrate reduction to ammonium). In the oxidative environment at the downstream transect, the subprocess of NH_4^+ → NO_2^- exceeded that of NO_2^- → NO_3^- in nitrification. All the above-mentioned processes can lead to the accumulation of NO_2^- at the two transects. Since the main aim of this study is to quantify the water exchange rates and associated chemical fluxes, we have not conducted the study on biogeochemical reactions. Whilst, further study could be done to explore the potential reasons in the future.

5. Conclusions

This study quantitatively evaluated the groundwater-surface water exchanges and associated nutrient fluxes along an upstream mangrove swamp transect and a downstream bare tidal flat transect, Dan'ao Estuary, China. We find that the SGDs, Inflows and fresh groundwater, river water, seawater fractions in intertidal groundwater along the two transects are significantly different from each other. Higher groundwater-surface water exchange rates show a great potential to decrease the salinity and increase the nutrient concentrations in intertidal groundwater. The great fresh groundwater recharge at the upstream transect can raise its fraction in intertidal groundwater and drive its nitrogen forms to be more reductive (i.e. relatively high concentrations of NH_4^+). These two aspects are beneficial to the mangrove growths at the upstream transect. The mangrove swamp with a substantial SGD, in return, serves as a vital source of abundant nutrients to the surface waters in this estuary. On the contrary, at the downstream transect, the much lower water exchange rates, higher salinities and lower nutrient concentrations lead to its very limited nutrient fluxes through the water-sediment interfaces. Moreover, the net nutrient loads to the sea by water exchange in the estuary section between the two transects are comparable to those by the local river discharge.

The results provide quantitative information on the groundwater-surface water exchanges and associated nutrient fluxes at the two intertidal transects in the typical tidal wetland at Dan'ao Estuary. Whereas the field observations are relatively short-term in the dry season, the long-term, maybe at least a spring-neap tide cycle, dynamics of the water and associated nutrient exchanges with tides in different seasons should be further studied in the future. Besides, efforts on larger-scale monitoring transects and extents of study areas are expected to gain more rational assessments.

Acknowledgements

The research is financially supported by the National Basic Research Program of China ("973" Program, Grant no. 2015CB452902), the Key program of National Natural Science Foundation of China (Grant no. 41430641) and Shenzhen Municipal Science and Technology Innovation Committee through project Shenzhen Key Laboratory of Soil and Groundwater Pollution Control (No. ZDSY20150831141712549). We appreciate Yanman Li, Shuaishuai Liu, Xiaolang Zhang, Meng Zhang, An An, Tiao Guo, Kanghan Zhou, Liang Zhong and Lijia Hou for their field work and laboratory experiment.

Declarations of interest

None.

Contributors

Gang Li and Hailong Li organized and conducted the study design, performed the statistical analysis and drafted the manuscript. Xuejing Wang. Wenjing Qu and Yan Zhang contributed to the data analyses and language improvements. Kai Xiao and Manhua Luo contributed to the study design and laboratory experiments. Chunmiao Zheng checked the data, figures and improved language. All the authors approved the final article.

Appendix A. Supplementary material

Supplementary data associated with this article can be found in the online version at doi:10.1016/j.csr.2018.06.014.

References

Akamatsu, Y., Ikeda, S., Toda, Y., 2009. Transport of nutrients and organic matter in a mangrove swamp. Estuar. Coast. Shelf Sci. 82, 233–242.

An, S.M., Gardner, W.S., 2002. Dissimilatory nitrate reduction to ammonium (DNRA) as a nitrogen link, versus denitrification as a sink in a shallow estuary (Laguna Madre/Baffin Bay, Texas). Mar. Ecol. Prog. Ser. 237, 41–50.

Burnett, W.C., Taniguchi, M., Oberdorfer, J., 2001. Measurement and significance of the direct discharge of groundwater into the coastal zone. J. Sea Res. 46, 109–116.

Charette, M.A., 2007. Hydrologic forcing of submarine groundwater discharge: insight from a seasonal study of radium isotopes in a groundwater-dominated salt marsh estuary. Limnol. Oceanogr. 52, 230–239.

Charette, M.A., Buesseler, K.O., 2004. Submarine groundwater discharge of nutrients and copper to an urban subestuary of Chesapeake bay (Elizabeth River). Limnol. Oceanogr. 49, 376–385.

Charette, M.A., Henderson, P.B., Breier, C.F., Liu, Q., 2013. Submarine groundwater discharge in a river-dominated Florida estuary. Mar. Chem. 156, 3–17.

Ganju, N.K., 2011. A novel approach for direct estimation of fresh groundwater discharge to an estuary. Geophys. Res. Lett. 38, 1–6.

Garrison, G.H., Glenn, C.R., McMurtry, G.M., 2003. Measurement of submarine groundwater discharge in Kahana Bay, O'ahu, Hawai'i. Limnol. Oceanogr. 48, 920–928.

Giblin, A.E., Gaines, A.G., 1990. Nitrogen inputs to a marine embayment – the importance of groundwater. Biogeochemistry 10, 309–328.

Gleeson, J., Santos, I.R., Maher, D.T., Golsby-Smith, L., 2013. Groundwater–surface water exchange in a mangrove tidal creek: evidence from natural geochemical tracers and implications for nutrient budgets. Mar. Chem. 156, 27–37.

Harvey, J.W., Odum, W.E., 1990. The influence of tidal marshes on upland groundwater discharge to estuaries. Biogeochemistry 10, 217–236.

Hou, L.J., Li, H.L., Zheng, C.M., Ma, Q., Wang, C.Y., Wang, X.J., Qu, W.J., 2016. Seawater-groundwater exchange in a silty tidal flat in the south coast of Laizhou Bay, China. J. Coast. Res. 74, 136–148.

Hwang, D.W., Lee, I.S., Choi, M., Kim, T.H., 2016. Estimating the input of submarine groundwater discharge (SGD) and SGD-derived nutrients in Geoje Bay, Korea using Rn-222-Si mass balance model. Mar. Pollut. Bull. 110, 119–126.

Hwang, D.W., Lee, Y.W., Kim, G., 2005. Large submarine groundwater discharge and benthic eutrophication in Bangdu Bay on volcanic Jeju Island, Korea. Limnol. Oceanogr. 50, 1393–1403.

Ji, T., Du, J.Z., Moore, W.S., Zhang, G.S., Su, N., Zhang, J., 2013. Nutrient inputs to a Lagoon through submarine groundwater discharge: the case of Laoye Lagoon, Hainan, China. J. Mar. Syst. 111, 253–262.

Krest, J.M., Moore, W.S., Gardner, L.R., Morris, J.T., 2000. Marsh nutrient export supplied by groundwater discharge: evidence from radium measurements. Glob. Biogeochem. Cycles 14, 167–176.

Kroeger, K.D., Swarzenski, P.W., Greenwood, W.J., Reich, C., 2007. Submarine groundwater discharge to Tampa Bay: nutrient fluxes and biogeochemistry of the coastal aquifer. Mar. Chem. 104, 85–97.

Liu, J.A., Su, N., Wang, X.L., Du, J.Z., 2017. Submarine groundwater discharge and associated nutrient fluxes into the Southern Yellow Sea: a case study for semi-enclosed and oligotrophic seas-implication for green tide bloom. J. Geophys. Res.: Oceans 122, 139–152.

Luo, X., Jiao, J.J., 2016. Submarine groundwater discharge and nutrient loadings in Tolo Harbor, Hong Kong using multiple geotracer-based models, and their implications of red tide outbreaks. Water Res. 102, 11–31.

Ma, Q., Li, H.L., Wang, X.J., Wang, C.Y., Wan, L., Wang, X.S., Jiang, X.W., 2015. Estimation of seawater–groundwater exchange rate: case study in a tidal flat with a large-scale seepage face (Laizhou Bay, China). Hydrogeol. J. 23, 265–275.

Millero, F.J., 2013. Chemical Oceanography, 4th ed. Taylor & Francis, Boca Raton.

Moore, W.S., 1999. The subterranean estuary: a reaction zone of ground water and sea water. Mar. Chem. 65, 111–125.

Moore, W.S., Krest, J., Taylor, G., Roggenstein, E., Joye, S., Lee, R., 2002. Thermal evidence of water exchange through a coastal aquifer: implications for nutrient fluxes. Geophys. Res. Lett. 29, 1–4.

Pilson, M.E.Q., 1998. An Introduction to the Chemistry of the Sea. Prentice Hall, Upper Saddle River, N.J.

Portnoy, J.W., Nowicki, B.L., Roman, C.T., Urish, D.W., 1998. The discharge of nitrate-contaminated groundwater from developed shoreline to marsh-fringed estuary. Water Resour. Res. 34, 3095–3104.

Qu, W.J., Li, H.L., Huang, H., Zheng, C.M., Wang, C.Y., Wang, X.J., Zhang, Y., 2017. Seawater-groundwater exchange and nutrients carried by submarine groundwater discharge in different types of wetlands at Jiaozhou Bay, China. J. Hydrol. 555, 185–197.

Reef, R., Feller, I.C., Lovelock, C.E., 2010. Nutrition of mangroves. Tree Physiol. 30, 1148–1160.

Ren, X.W., Jiang, G.Q., Liu, A.P., Li, K.M., 2013. Estimation of main river pollution fluxes into Daya Bay. In: Proceedings of the Annual Conference of Chinese Society for Environmental Sciences. Kunming, Yunnan, China. (in Chinese).

Rengarajan, R., Sarma, V.V.S.S., 2015. Submarine groundwater discharge and nutrient addition to the coastal zone of the Godavari estuary. Mar. Chem. 172, 57–69.

Russoniello, C.J., Fernandez, C., Bratton, J.F., Banaszak, J.F., Krantz, D.E., Andres, A.S., Konikow, L.F., Michael, H.A., 2013. Geologic effects on groundwater salinity and discharge into an estuary. J. Hydrol. 498, 1–12.

Sadat-Noori, M., Santos, I.R., Tait, D.R., Reading, M.J., Sanders, C.J., 2017. High pore-water exchange in a mangrove-dominated estuary revealed from short-lived radium isotopes. J. Hydrol. 553, 188–198.

Sakamaki, T., Nishimura, O., Sudo, R., 2006. Tidal time-scale variation in nutrient flux across the sediment–water interface of an estuarine tidal flat. Estuar. Coast. Shelf Sci. 67, 653–663.

Slomp, C.P., Van Cappellen, P., 2004. Nutrient inputs to the coastal ocean through submarine groundwater discharge: controls and potential impact. J. Hydrol. 295, 64–86.

State Oceanic Administration of the People's Republic of China, 2007. Specification for Marine Monitoring, Part 4: Seawater Analysis. General Administration of Quality Supervision, Inspection and Quarantine & Standardization Administration of the People's Republic of China, Beijing, China (in Chinese).

Taniguchi, M., Burnett, W.C., Cable, J.E., Turner, J.V., 2002. Investigation of submarine groundwater discharge. Hydrol. Process. 16, 2115–2129.

Valiela, I., Costa, J., Foreman, K., Teal, J.M., Howes, B., Aubrey, D., 1990. Transport of groundwater-borne nutrients from watersheds and their effects on coastal waters. Biogeochemistry 10, 177–197.

Wang, X., Li, H., Zheng, C., Yang, J., Zhang, Y., Zhang, M., Qi, Z., Xiao, K., Zhang, X., 2018. Submarine groundwater discharge as an important nutrient source influencing nutrient structure in coastal water of Daya Bay, China. Geochim. Cosmochim. Acta 225, 52–65.

Wang, X.J., Li, H.L., Yang, J.Z., Wan, L., Wang, X.S., Jiang, X.W., Guo, H.M., 2014. Measuring in situ vertical hydraulic conductivity in tidal environments. Adv. Water Resour. 70, 118–130.

Wilson, A.M., Morris, J.T., 2012. The influence of tidal forcing on groundwater flow and nutrient exchange in a salt marsh-dominated estuary. Biogeochemistry 108, 27–38.

Wu, W., Yan, Y.H., Song, D.H., 2017. Study on the tidal dynamics in Daya Bay, China Part I. Observation and numerical simulation of tidal dynamic system. Chin. J. Trop. Oceanogr. 36, 34–45 (in Chinese).

Xia, Y.Q., Li, H.L., 2012. A combined field and modeling study of groundwater flow in a tidal marsh. Hydrol. Earth Syst. Sci. 16, 741–759.